

A NOZZLE ANALYSIS OF SLOW-ACCELERATION SOLUTIONS IN ONE-DIMENSIONAL MODELS OF ROTATING HOT-STAR WINDS

THOMAS I. MADURA AND STANLEY P. OWOCKI

Bartol Research Institute, Department of Physics and Astronomy, University of Delaware, Newark, DE 19716;
tmadura@udel.edu, owocki@bartol.udel.edu

AND

ACHIM FELDMEIERS

Astrophysik, Institut für Physik, Universität Potsdam, Am Neuen Palais 10, 14469 Potsdam, Germany; afeld@astro.physik.uni-potsdam.de
Received 2006 September 1; accepted 2007 January 8

ABSTRACT

One-dimensional (1D) stellar wind models for hot stars rotating at $\geq 75\%$ of the critical rate show a sudden shift to a slow-acceleration mode, implying a slower, denser equatorial outflow that might be associated with the dense equatorial regions inferred for B[e] supergiants. Here we analyze the steady 1D flow equations for a rotating stellar wind based on a “nozzle” analogy for terms that constrain the local mass flux. For low rotation, we find the nozzle minimum occurs near the stellar surface, allowing a transition to a standard, CAK-type steep-acceleration solution; but for rotations $\geq 75\%$ of the critical rate, this inner nozzle minimum exceeds the global minimum, implying near-surface supercritical solutions would have an overloaded mass-loss rate. In steady, analytic models in which the acceleration is assumed to be monotonically positive, this leads the solution to switch to a slow-acceleration mode. However, time-dependent simulations using a numerical hydrodynamics code show that, for rotation rates 75%–85% of critical, the flow can develop abrupt “kink” transitions from a steep acceleration to a *decelerating* solution. For rotations above 85% of critical, the hydrodynamic simulations confirm the slow acceleration, with the lower flow speed implying densities 5–30 times higher than the polar (or a nonrotating) wind. Still, when gravity darkening and 2D flow effects are accounted for, it seems unlikely that rotationally modified equatorial wind outflows could account for the very large densities inferred for the equatorial regions around B[e] supergiants.

Subject headings: hydrodynamics — stars: early-type — stars: emission-line, Be — stars: mass loss — stars: rotation — stars: winds, outflows

1. INTRODUCTION

Hot, luminous, massive stars of spectral types O and B are generally quite rapid rotators, with inferred surface rotation speeds typically in the range of several hundred kilometers per second, or a substantial fraction of the critical rotation speed (ca. 400–600 km s⁻¹) at which material at the rotating equatorial surface would be in Keplerian orbit. Such luminous stars are also characterized by strong stellar wind outflows, driven by the line scattering of the star’s continuum radiation flux (Castor et al. 1975, hereafter CAK). A long-standing question is how such wind outflows are affected by the star’s rotation and in particular whether this might play a role in the enhanced equatorial density outflows and/or disks inferred in certain classes of particularly rapid rotators, e.g., Be and B[e] stars.

For classical Be stars, there is now substantial observational evidence (see, e.g., papers in Ignace & Gayley 2005) that the disks are Keplerian in nature, with very limited radial outflow; they are thus probably *not* a direct result of feeding by a steady stellar wind (Owocki 2005). However, for the disk and/or enhanced equatorial outflows inferred in supergiant B[e] stars, wind mechanisms still seem a viable option. For example, Lamers & Pauldrach (1991) and Pelupessy et al. (2000) have noted that the “bistability” enhancement in opacity which occurs for some value of the local surface effective temperature (i.e., for B-type stars at $\sim 22,000$ K; see Pauldrach & Puls 1990; Vink et al. 1999) associated with the reduced radiation temperature near the equator can lead to a factor of several enhancement in the radial mass flux. By itself, this seems inadequate to explain equatorial densi-

ties estimated to be hundreds or even thousands of times the densities of the polar winds in these stars (Zickgraf et al. 1985; Kraus & Miroshnichenko 2006). However, a recent series of papers by M. Curé and colleagues (Curé 2004; Curé & Rial 2004; Curé et al. 2005) proposes that, for very high, near-critical rotation, a switch of the wind outflow to a slower, shallow-acceleration solution can lead to a further enhancement in density that, together with the bistability effect, might reach the equatorial densities inferred in B[e] supergiants.

This paper aims to understand better the physical origin of these shallow wind acceleration solutions for high rotation rates and to examine critically their likely relevance for explaining dense equatorial disks or outflows.

Modeling rotating, hot-star winds began with the studies by Friend & Abbott (1986, hereafter FA86) and by Pauldrach et al. (1986, hereafter PPK86), who extended the CAK formalism by adding the effect of an outward centrifugal acceleration to one-dimensional (1D) models of the wind outflow in the equatorial plane. Both FA86 and PPK86 independently derived a modified CAK model (mCAK) that relaxes the CAK “point star” approximation and properly accounts for the finite cone angle subtended by the star. They each then found that the reduction in the effective gravity by the outward centrifugal force tends to increase the mass-loss rate and decrease the wind speed. However, for the models computed, up to about 75% of the critical rotation rate, both changes are limited to only a factor of a few and are thus insufficient to produce the large equatorial densities and low velocities inferred in B[e] supergiants. Moreover, for still faster rotation, above about 75% critical, FA86 found that the equations for

outward acceleration could no longer be integrated beyond some finite radius, and thus they were unable to derive any complete flow solutions for such rapid rotation speeds. Subsequent 1D models have investigated the role of magnetic forces (Friend & MacGregor 1984; Poe & Friend 1986) and sound waves (Koninx & Hearn 1992), but as summarized by Bjorkman & Cassinelli (1993) neither mechanism seems favorable for producing slow, dense equatorial outflows.

More fundamentally, the physical relevance of any such 1D models may be limited since accounting for latitudinal flows toward or away from the equator requires at least a two-dimensional (2D) treatment. A vivid example comes from the 2D “wind-compressed disk” (WCD) model of Bjorkman & Cassinelli (1993), which argues that conservation of angular momentum should tend to channel material from higher latitudes toward an equatorially compressed disk flow. If one assumes a purely radial driving force, 2D hydrodynamic simulations (Owocki et al. 1994) confirm the basic WCD effect but show that, depending on whether material reaches the equator above or below some “stagnation point,” it either drifts outward or falls back toward the star. Such simultaneous infall-plus-outflow behavior is not possible in a steady 1D model but is a perfectly natural outcome in a 2D simulation. Furthermore, Cranmer & Owocki (1995) showed that, when computed from proper angle integration of intensity from the rotationally distorted stellar surface, the line force also has nonzero, *nonradial* components in both azimuth and latitude. Owocki et al. (1996; see also Petrenz & Puls 2000) showed that such nonradial line forces can *inhibit* the formation of a WCD. Finally, equatorial gravity darkening can actually *reduce* the wind mass flux from the equator and so lead to an equatorial wind density that is *lower*, not higher, than near the poles.

Despite this likely importance of such 2D effects, several recent analyses (Curé 2004; Curé & Rial 2004; Curé et al. 2005) have reexamined the 1D equatorial flow models of FA86, with a particular focus on the failure to obtain monotonically accelerating wind solutions for rotation above about 75% of the critical speed. In particular, these papers argue that for such very high, near-critical rotation, the wind solution can switch to an alternative mode, characterized by a much *slower* outward acceleration. Together with a moderately enhanced mass flux, the resulting lower speed outflow then implies a substantial enhancement in density, relative to the standard CAK, steep acceleration applicable at higher latitudes. When combined with parameterizations intended to mimic a bistability enhancement in the line driving (Lamers & Pauldrach 1991; Pelupessy et al. 2000), Curé et al. (2005) predict equator-to-pole density contrasts of the order of 10^2 – 10^4 .

Assessing the physical relevance of such claims for understanding B[e] stars will eventually require proper account of the multidimensional effects noted above. Nonetheless, to provide a solid basis for such multidimensional models, it is important to have a clearer, dynamical understanding of these novel 1D slow-outflow solutions. By combining analytic studies with numerical hydrodynamic simulations, this paper examines the reality and physical origin of the shallow wind acceleration solutions for high rotation rates, with emphasis on their possible relevance to disk outflows from B[e] supergiants.

We begin (§ 2) with a basic review of the general time-dependent wind equations, together with their CAK-type, steady state solutions in a nonrotating wind. To provide a physical basis for extending these steady models to include rotation, we first (§ 3) apply a simple “nozzle” analysis (see Holzer 1977; Abbott 1980), originally developed to study winds driven from luminous accretion disks (Pereyra et al. 2004). With a few judicious, yet

quite reasonable, approximations (e.g., neglecting gas pressure terms by taking the zero sound-speed limit, using a beta velocity law to evaluate the finite-disk correction as an explicit function of radius), it is possible to obtain simple integrations of the equation of motion and to study the scalings of the mass-loss rate with rotation, as well as the switch from steep- to shallow-acceleration solutions beyond a threshold rotation rate. To test the validity of these simple analytic solutions, we next apply a numerical hydrodynamics code (§ 4) to evolve 1D rotating wind models to asymptotic steady states (§ 5.1). Results confirm a transition to slower acceleration at very high rotation (above about 85% of critical) but also show a new class of nonmonotonic “kink” solutions that apply for moderately fast rotation (ca. 75%–85% of critical). We then examine (§§ 5.2–5.3) the time evolution of solutions in various rotation domains, with emphasis on the kink solutions and on a peculiar transition case (85% of critical rotation), characterized by an initial wind overloading followed by a flow stagnation and eventual reaccretion of material onto the star. We conclude with a summary and outlook for future work (§ 6).

2. GENERAL FORMALISM FOR LINE-DRIVEN MASS LOSS

2.1. 1D Time-dependent Equations of Motion

In this paper, we examine 1D radiatively driven outflow in the equatorial plane of a rotating star. For the general time-dependent simulations discussed in § 3, the relevant equations for conservation of mass and radial component of momentum have the form

$$\frac{\partial \rho}{\partial t} + \frac{1}{r^2} \frac{\partial (r^2 \rho v)}{\partial r} = 0, \quad (1)$$

$$\frac{\partial v}{\partial t} + v \frac{\partial v}{\partial r} = \frac{v_\phi^2}{r} - \frac{1}{\rho} \frac{\partial P}{\partial r} - \frac{GM_*(1 - \Gamma_e)}{r^2} + g_{\text{lines}}, \quad (2)$$

where r and t are the radius and time, and ρ and v are the mass density and radial component of the velocity. The body forces here include the outward radiative acceleration from line scattering, g_{lines} , and an effective inward gravitational acceleration, $GM_*(1 - \Gamma_e)/r^2$, reduced by the outward continuum radiative force from scattering by free electrons, as accounted for by the Eddington parameter, $\Gamma_e = \kappa_e L_*/4\pi GM_*c$. For the centrifugal term, v_ϕ^2/r , we avoid explicit treatment of an azimuthal momentum equation by assuming simple angular momentum conservation (which is a good approximation in the supersonic flow domain considered here), yielding then for the azimuthal speed

$$v_\phi = v_{\text{rot}} \frac{R_*}{r}, \quad (3)$$

where v_{rot} is the rotation speed at the star’s equatorial surface radius R_* . For simplicity, we also avoid a detailed treatment of the wind energy balance by assuming an isothermal outflow, for which the pressure is written as $P = \rho a^2$, where a is the (constant, isothermal) sound speed.

2.2. Steady State Equations with Rotation

For the simplified case of a steady state, the time-dependent terms vanish ($\partial/\partial t = 0$), yielding for the steady acceleration

$$v \frac{dv}{dr} = - \frac{GM_*(1 - \Gamma_e)}{r^2} + \frac{v_{\text{rot}}^2 R_*^2}{r^3} + g_{\text{lines}} - \frac{a^2}{\rho} \frac{d\rho}{dr}. \quad (4)$$

The steady form for mass conservation implies a constancy for the overall mass-loss rate, $\dot{M} \equiv 4\pi\rho v r^2$. Using this to eliminate the density ρ , the equation of motion (4) takes the form

$$\left[1 - \frac{a^2}{v^2}\right] v \frac{dv}{dr} = -\frac{GM_*(1 - \Gamma_e)}{r^2} + \frac{v_{\text{rot}}^2 R_*^2}{r^3} + g_{\text{lines}} + \frac{2a^2}{r}. \quad (5)$$

The factor in square brackets on the left-hand side allows for a smooth mapping of the wind base onto a hydrostatic atmosphere below the sonic point, where $v < a$. However, in radiatively driven winds the pressure terms on the right-hand side are generally negligible since, compared to the gravitational acceleration term that must be overcome to drive a wind, these are of order $w_s \equiv (a/v_{\text{esc}})^2 \approx 0.001$, where $v_{\text{esc}} \equiv [2GM_*(1 - \Gamma_e)/R_*]^{1/2}$ is the effective escape speed from the stellar surface radius R_* .

Since the key to a stellar wind is overcoming gravity, it is convenient to define a dimensionless equation of motion that scales all accelerations by the effective gravity,

$$\left(1 - \frac{w_s}{w}\right) w' = -1 + \omega^2(1 - x) + \Gamma_{\text{lines}} + \frac{4w_s}{1 - x}, \quad (6)$$

where $\Gamma_{\text{lines}} \equiv g_{\text{lines}} r^2 / GM_*(1 - \Gamma_e)$, and the gravitationally scaled inertia is $w' \equiv dw/dx = r^2 v (dv/dr) / GM_*(1 - \Gamma_e)$. The independent variable here is the inverse radius coordinate $x \equiv 1 - R_*/r$, while the dependent variable is the ratio of the radial kinetic energy to the effective surface escape energy, $w \equiv v^2/v_{\text{esc}}^2$. Gas pressure effects are accounted for by terms containing $w_s \equiv a^2/v_{\text{esc}}^2$, while centrifugal effects from rotation are characterized in terms of the ratio of the equatorial rotation speed to critical speed, $\omega \equiv v_{\text{rot}}/v_{\text{crit}} = \sqrt{2}v_{\text{rot}}/v_{\text{esc}}$, under the assumption that the wind material conserves its surface value of specific angular momentum, $rv_\phi(r) = v_{\text{rot}}R_*$.

Within the CAK formalism for driving by scattering of a point source of radiation by an ensemble of lines, the deshadowing of optically thick lines by the Doppler shift associated with the wind acceleration gives the scaled radiative acceleration Γ_{lines} a power-law dependence on the flow acceleration w' ,

$$\Gamma_{\text{lines}} = Cw'^\alpha, \quad (7)$$

where α is the CAK power index. Here we have eliminated an inverse dependence on density ρ in favor of the mass-loss rate $\dot{M} = 4\pi r^2 \rho v$, with the line force constant thus defined by

$$C \equiv \frac{1}{1 - \alpha} \left(\frac{L_*}{\dot{M}c^2}\right)^\alpha \left(\frac{\bar{Q}\Gamma_e}{1 - \Gamma_e}\right)^{1-\alpha}, \quad (8)$$

with L_* the stellar luminosity and Γ_e the Eddington parameter for the gravitationally scaled radiative acceleration from electron scattering opacity, κ_e (in square centimeters per gram; Lamers & Cassinelli 1999; Owocki 2004). We have also used the Gayley (1995) \bar{Q} notation for the overall normalization of the line opacity. Note that, for fixed sets of stellar parameters (L_* , M_* , Γ_e) and line opacity (α , \bar{Q}), the constant C scales with the mass-loss rate as $C \propto 1/\dot{M}^\alpha$.

As already noted, the smallness of the dimensionless sound-speed parameter w_s implies that gas pressure plays little role in the dynamics of any line-driven stellar wind. Hence, to a good approximation, we can obtain accurate solutions by analyzing the much simpler limit of vanishing sound speed $a \propto w_s^{1/2} \rightarrow 0$, for which the line-driven wind equation of motion reduces to

$$w' = -1 + \omega^2(1 - x) + Cw'^\alpha. \quad (9)$$

2.3. Classical CAK Solution for a Point Star

Let us first review the standard CAK solution without rotation, setting $\omega = 0$. Note then that since the parameters Γ_e and C are spatially constant, the solution is independent of radius. For high \dot{M} and small C there are no solutions, while for small \dot{M} and high C there are two solutions. The CAK *critical* solution (denoted by the subscript c) corresponds to a *maximal* mass-loss rate, which requires a *tangential* intersection between the line force Cw'^α and the combined inertia plus gravity $1 + w'$, for which

$$\alpha C_c w_c'^{\alpha-1} = 1, \quad (10)$$

and thus, together with the equation of motion (9), we have

$$w_c' = \frac{\alpha}{1 - \alpha}, \quad (11)$$

with

$$C_c = \frac{1}{\alpha^\alpha (1 - \alpha)^{1-\alpha}}. \quad (12)$$

Using equation (8), this then yields the standard CAK scaling for the mass-loss rate,

$$\dot{M}_{\text{CAK}} = \frac{L_*}{c^2} \frac{\alpha}{1 - \alpha} \left(\frac{\bar{Q}\Gamma_e}{1 - \Gamma_e}\right)^{(1-\alpha)/\alpha}. \quad (13)$$

Moreover, since the scaled equation of motion (9) has no explicit spatial dependence, the scaled critical acceleration w_c' applies throughout the wind. This can therefore be trivially integrated to yield

$$w(x) = w(1)x, \quad (14)$$

where $w(1) = \alpha/(1 - \alpha)$ is the terminal value of the scaled flow energy. In terms of dimensional quantities, this represents a specific case of the general beta velocity law,

$$v(r) = v_\infty \left(1 - \frac{R_*}{r}\right)^\beta, \quad (15)$$

where in this case $\beta = \frac{1}{2}$, and the wind terminal speed scales with the effective escape speed from the stellar surface, $v_\infty = v_{\text{esc}}[\alpha/(1 - \alpha)]^{1/2}$.

2.4. Finite-Disk Form for the CAK Line Force

The above analysis is based on the idealization of radially streaming radiation, as if the star were a point source at the origin. This was the basis of the original CAK wind solutions, although they did already identify (but did not implement) the appropriate “finite-disk correction factor” (FDCF) to account for the full angular extent of the star (see Castor et al. 1975, eq. [50]),

$$f(r) = \frac{(1 + \sigma)^{1+\alpha} - (1 + \sigma\mu_*^2)^{1+\alpha}}{(1 + \alpha)\sigma(1 + \sigma)^\alpha(1 - \mu_*^2)}, \quad (16)$$

with $\mu_* \equiv (1 - R_*^2/r^2)^{1/2}$ the cosine of the finite cone angle of the stellar disk and $\sigma \equiv d \ln v / d \ln r - 1$. When this factor is included to modify the point-star CAK line acceleration (from eq. [7]), its complex dependence on radius, velocity, and velocity gradient complicates the solution of the full equation of motion. Full solutions derived independently by FA86 and PPK86 yield a

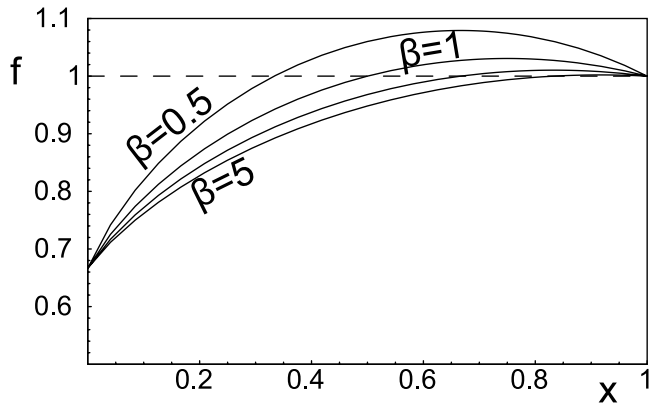


FIG. 1.—Spatial variation of the FDCF f vs. scaled inverse radius $x = 1 - R_*/r$ for CAK exponent $\alpha = \frac{1}{2}$ and various velocity-law exponents, $\beta = 0.5, 1, 2,$ and 5 . The horizontal dashed line denotes the unit correction that applies at the point of isotropic expansion (where $\sigma = d \ln v / d \ln r - 1 = 0$) and at large distances where the star approaches the point-source form assumed in the original CAK model.

somewhat reduced mass-loss rate $\dot{M}_{\text{fd}} \approx \dot{M}_{\text{CAK}} / (1 + \alpha)^{1/\alpha}$ and higher terminal speed $v_\infty \approx 3v_{\text{esc}}$.

But if we approximate the wind velocity law by the simple beta-law form of equation (15), then the FDCF can be evaluated as an *explicit* spatial function. Figure 1 illustrates the resulting variation of f with the scaled coordinate x for $\alpha = \frac{1}{2}$ and various values of β . Note that the overall form is quite similar for all cases, increasing from a surface value $f_* \equiv f(R_*) = 1/(1 + \alpha)$ to past unity at the isotropic expansion radius (where $dv/dr = v/r$), $r/R_* = (1 + \beta)$ [corresponding to $x = \beta/(1 + \beta)$], and eventually returning asymptotically to unity from above at large radii ($x \rightarrow 1$).

In the steady wind analysis in the next section, we thus choose the canonical value $\beta = 1$ to represent the FDCF as an explicit spatial function (PPK86).

3. STEADY STATE SOLUTIONS FOR 1D MODELS OF ROTATING, LINE-DRIVEN STELLAR WINDS

3.1. Nozzle Analysis for Steady Wind Acceleration

Let us now examine how the combined effects of the FDCF and rotation alter the classical CAK result. Note that we are ignoring here gravity darkening and oblateness effects, as well as any bistability in the line-driving parameters between the polar and equatorial wind. For a rotating star and wind, the FDCF can become even more complicated, modified by the rotational shear of the wind outflow and by the oblateness of the star, and possibly also by the equatorial gravity darkening of the source radiation (Cranmer & Owocki 1995; Gayley & Owocki 2000). However, for simplicity, let us nonetheless base our analysis on the spatially explicit form obtained by assuming a canonical $\beta = 1$ velocity law (15) within finite-disk factor (16) for a simple spherical expansion. In the zero sound-speed limit, the scaled equation of motion (9) can now be written in the form

$$w' = -1 + \omega^2(1 - x) + f C_c \left(\frac{w'}{\dot{m}} \right)^\alpha, \quad (17)$$

where we have normalized the line force in terms related to the point star CAK model, with $\dot{m} \equiv \dot{M}/\dot{M}_{\text{CAK}}$, the ratio of the mass-loss rate to the point-star CAK value. Note then that for the non-rotating ($\omega = 0$), point-star ($f = 1$) case of the classical CAK model, the critical solution (with maximal mass loss) is given by

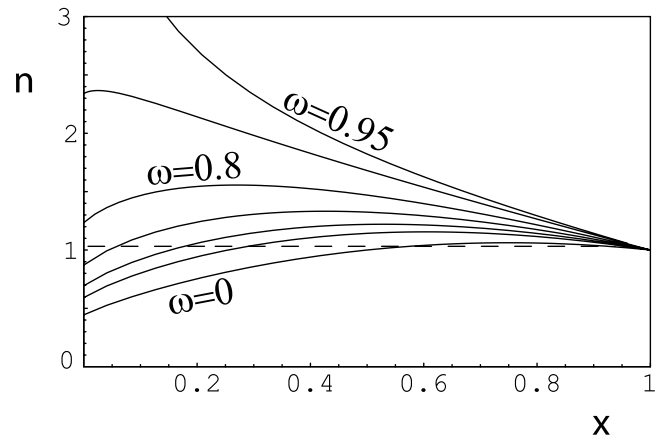


FIG. 2.—Nozzle function $n(x)$ vs. scaled inverse radius $x = 1 - R_*/r$ for various rotation rates $\omega = 0, 0.5, 0.6, 0.7, 0.8, 0.9,$ and 0.95 , ranging from lowermost to uppermost. All curves use a $\beta = 1$ velocity law in evaluating the FDCF. The horizontal dashed line at unit value represents the nozzle function for the CAK point-star model, with $n = f = g = 1$.

$\dot{m} = 1$ and $w(x) = \alpha/(1 - \alpha)x$. As noted in § 2.3, this implies a CAK mass-loss rate $\dot{M} = \dot{M}_{\text{CAK}}$ and a velocity law $v(r) = v_\infty(1 - R_*/r)^{1/2}$, with terminal speed $v_\infty = [\alpha/(1 - \alpha)]^{1/2}v_{\text{esc}}$.

To analyze models with rotation, a particularly convenient case is to take $\alpha = \frac{1}{2}$, for which the equation of motion (17) (using eq. [12] for C_c) becomes a simple quadratic in $(w')^{1/2}$,

$$w' - 2f \sqrt{\frac{w'}{\dot{m}}} + g(x) = 0, \quad (18)$$

where for convenience we have defined a rotationally reduced gravity as $g(x) \equiv 1 - \omega^2(1 - x)$. We can then solve for a shallow (−) and steep (+) acceleration solution,

$$w'_\pm(x) = \frac{g(x)n(x)}{\dot{m}} \left[1 \pm \sqrt{1 - \frac{\dot{m}}{n(x)}} \right]^2, \quad (19)$$

with the “nozzle function,”

$$n(x) \equiv \frac{f(x)^2}{g(x)} = \frac{f(x)^2}{1 - \omega^2(1 - x)}. \quad (20)$$

The significance of this nozzle function stems from its appearance with the mass-loss rate \dot{m} within the square-root discriminant (cf. de Laval nozzle; Abbott 1980). In particular, we can readily see that maintaining a numerically real flow acceleration requires¹ a mass-loss rate $\dot{m} \leq \min[n(x)]$. As such, the location of the global minimum of this function (the smallest nozzle “throat”) represents the *critical point* that sets the maximal allowed value of the mass-loss rate, $\dot{m} = \min[n(x)]$, that is consistent with a monotonically accelerating outflow.

Figure 2 plots $n(x)$ versus x for various rotation rates ω , using a $\beta = 1$ velocity law to obtain a spatially explicit approximation to the FDCF. Note that for no or low rotation (about $\omega < 0.75$), the minimum of the nozzle function is less than unity and occurs at the stellar surface, $x = 0$. This allows the flow to transition to a

¹ Actually, this restriction really stems from our CAK scaling of the line force with w'^α [in this case $(w')^{1/2}$], which requires a strictly *positive* acceleration, $w' > 0$. But if we provide a backup scaling for negative accelerations, then “overloaded” situations, for which the square-root discriminant in eq. (19) becomes negative, simply lead to an abrupt switch, a so-called kink (Cranmer & Owocki 1996), to a *decelerating* solution. See §§ 4 and 6 for further details.

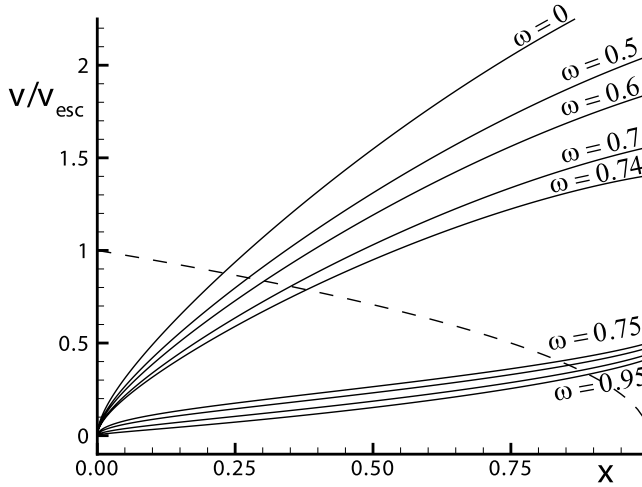


FIG. 3a

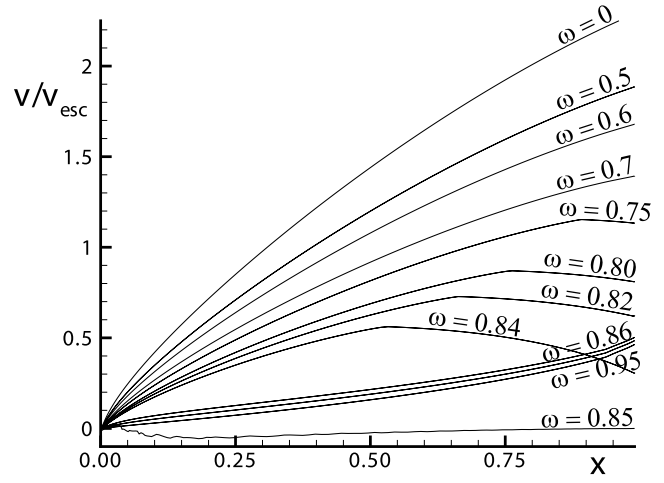


FIG. 3b

FIG. 3.—(a) Flow speed over escape speed, $v/v_{\text{esc}} = w^{1/2}$, vs. scaled inverse radius $x = 1 - R_s/r$, as derived from a nozzle analysis, using a steep acceleration for no or modest rotation, $\omega = 0, 0.5, 0.6, 0.7$, and 0.74 and shallow acceleration for rapid, near-critical rotation, $\omega = 0.75, 0.8, 0.85, 0.9$, and 0.95 . The dashed curve shows the escape speed as a function of x . (b) Same as (a), but as found using asymptotic states of full hydrodynamic simulations. Note again the steep, supercritical accelerations for no or modest rotation, $\omega = 0, 0.5$, and 0.7 , and shallow, subcritical accelerations for rapid, near-critical rotation, $\omega = 0.86, 0.9$, and 0.95 . However, note also the kink solutions present for $\omega = 0.75, 0.8, 0.82$, and 0.84 and the collapsed solution for $\omega = 0.85$.

supercritical outflow directly from the static surface boundary condition $w(0) = 0$, following the steeper, plus (+) root for the acceleration in equation (19), but with a mass-loss rate less than the point-star CAK value,

$$\dot{m} = \dot{m}_0 \equiv n(x=0) \equiv \frac{f^2(x=0)}{1-\omega^2} = \frac{4/9}{1-\omega^2}. \quad (21)$$

Note that the factor of $4/9$ in the numerator is just the $\alpha = \frac{1}{2}$ value for the zero-rotation, finite-disk corrected mass loss scaling derived by FA86 and PPK86,

$$\dot{m}_{\text{fd}} \equiv \frac{\dot{M}_{\text{fd}}}{\dot{M}_{\text{CAK}}} = f_*^{1/\alpha} = \frac{1}{(1+\alpha)^{1/\alpha}}. \quad (22)$$

By contrast, for large rotation rates (about $\omega > 0.75$), this nozzle minimum is unity and occurs at large radii, $x = 1$; satisfying the static surface boundary condition now implies that the flow at all finite radii should remain subcritical, following the shallower, minus (-) root for the acceleration in equation (19), now with a mass-loss rate just equal to the point-star CAK value, $\dot{m} = 1$.

This thus provides the basic explanation for the switch from steep to shallow accelerations inferred by Curé et al. (2005).

3.2. Nozzle Solutions for the Velocity Law in 1D Rotating Winds

The associated wind velocity laws can be obtained by simple numerical integration of equation (19) from a static boundary $w(0) = 0$, following either the steep or the shallow solution, depending on whether the rotation rate is high enough to shift the critical point [where $n(x)$ has its absolute minimum] from the surface ($x = 0$) to large radii ($x = 1$). Figure 3a plots the resulting velocity laws for selected slow versus rapid rotation rates, yielding the steep versus shallow types of flow solution, respectively. The dashed curve in Figure 3a plots the escape speed v_{esc} as a function of x , showing that these winds are capable of escaping

the star. Figure 3b compares results from full dynamical simulations described below.

Figure 4 illustrates the associated terminal speed and mass-loss rates for these solutions (solid lines), plotted as a function of rotation rate ω . As the rotation increases past the threshold rate at $\omega \approx 0.75$, the solid curves show an abrupt shift from steep acceleration to shallow acceleration, with the mass loss saturating to the point-star CAK value, $\dot{m} = 1$. The dashed curves show extrapolated results if the local nozzle minimum at the surface is instead used to set flow conditions; the mass loss in this case is set by the scaling \dot{m}_0 in equation (21), and the terminal speed is derived by assuming a pure gravitational coasting for all radii

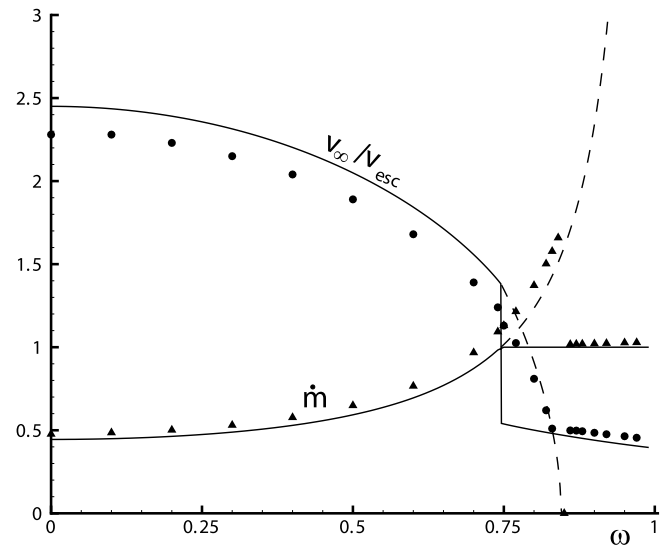


FIG. 4.—Upper solid curve: Terminal flow speed over escape speed, $v_{\infty}/v_{\text{esc}} = [w(1)]^{1/2}$, vs. rotation rate ω , showing the shift from fast to slow wind as rotation rate is increased past ca. $\omega = 0.75$. Lower solid curve: Mass-loss rate in units of point-star CAK value vs. rotation rate ω , showing the saturation at the CAK mass-loss rate for rapid rotation, $\omega > 0.75$. Dashed curves show the continued steady decrease in $v_{\infty}/v_{\text{esc}}$ and increase in \dot{m} if the local nozzle minimum at the stellar surface is used to set flow conditions (§ 3.2). The circles ($v_{\infty}/v_{\text{esc}}$) and triangles (\dot{m}) show corresponding results from full hydrodynamic simulations.

with $n(x) < \dot{m}_0$. The data points again compare corresponding results for the full dynamical simulation, as described further in the next sections.

4. SPECIFICATIONS FOR NUMERICAL HYDRODYNAMICS SIMULATIONS

The above nozzle analysis provides a helpful framework for understanding the nature of flow solutions from a rotating wind model but is based on some key simplifications, e.g., neglect of gas pressure (inclusion of which would lead to a wind that is not supercritical directly from the static surface boundary) and an approximate, spatially explicit form for the FDCF. Moreover, it implicitly assumes that the derived solutions are the only relevant stable, attracting steady states for the rotating wind outflow. To test the validity of these simplifications and assumptions, let us now examine the *time* evolution of analogous 1D flow models, also including both the finite gas pressure and the dynamically computed FDCF. Our specific approach here is to use a numerical hydrodynamics code to evolve a 1D time-dependent model of the equatorial plane for a line-driven stellar wind from a rotating star toward an equilibrium steady state for the resulting flow. The results of these simulations can then be compared to those predicted by the steady state nozzle analysis presented above.

The numerical models presented here were computed using a piecewise parabolic method (PPM; Collela & Woodward 1984) hydrodynamics code called VH-1, originally developed at the University of Virginia (J. Blondin). The basic code was modified for the present study to include radiative driving terms, solving the time-dependent equations for 1D spherical outflow equations (1) and (2). The spatial mesh uses $n_r = 600$ radial zones extending from the base at the stellar surface, $r_1 = R_{\min} = R_*$, to a maximum $r_{600} = R_{\max} = 100R_*$, with the zone spacing starting at $\Delta r_1 = 6.18 \times 10^{-5}R_*$ and then increasing by 2.5% per zone out to $r_{350} = 15R_*$, after which it remains constant at $\Delta r = 0.333R_*$ to the outer boundary. Tests with double the grid resolution for selected cases give similar results to the above standard values.

The parabolic method requires flow variables to be specified in a phantom zone beyond each boundary. At the outer radius, we assume supercritical outflow, with boundary conditions set by simple flow *extrapolation* assuming constant gradients. This is justified because, as discussed in the Appendix, when finite sound-speed terms are included, the critical point for even the shallow-acceleration solutions should be well within our assumed outer boundary radius of $R_{\max} = 100R_*$.

At the inner boundary, the velocity in the two radial zones below i_{\min} is set by constant-slope extrapolation, thus allowing the base velocity to adjust to whatever is appropriate for the overlying flow (Owocki et al. 1994). This usually corresponds to a subsonic wind outflow, although inflow at up to the sound speed is also allowed. The base density is fixed at $\rho_0 = 8.709 \times 10^{-13} \text{ g cm}^{-3}$, a value chosen because, for the characteristic wind mass fluxes of these models, it yields a steady base outflow that is moderately subsonic. A lower boundary density much smaller than this produces a base outflow that is supersonic and thus is unable to adjust properly to the mass flux appropriate to the overlying line-driven wind. On the other hand, a much larger base density makes the lower boundary too “stiff,” leading to persistent oscillations in the base velocity (Owocki et al. 1994).

These time-dependent simulations also require setting an *initial condition* for the density and velocity over the entire spacial mesh at some starting time $t = 0$. For this we generally use a standard, finite-disk corrected CAK wind, computed by relaxing a 1D, *nonrotating* simulation to a steady state; however, for selected models with moderately rapid rotation, we also explore

using a slow-acceleration initial condition (see § 5.3). From the assumed initial condition, the models are advanced forward in time steps set to a fixed fraction 0.25 of the Courant time.

Our version of VH-1 is set up to operate in cgs units, requiring specification of physical values for the basic parameters for both the star (e.g., mass, radius, and luminosity) and wind (e.g., CAK k , α , and δ). Building on our earlier studies of Be stars, the specific parameters chosen here are for a main-sequence B star with mass $M_* = 7.5 M_\odot$, radius $R_* = 4 R_\odot$, luminosity $L_* = 2310 L_\odot$, and temperature $T = 2 \times 10^4 \text{ K}$; but we have also explored models with parameters appropriate for supergiant B[e] stars. These stellar parameters imply an Eddington parameter of $\Gamma_e = 0.008$, an isothermal sound speed of $a = 16.6 \text{ km s}^{-1}$, and escape and critical speeds of $v_{\text{esc}} = 845 \text{ km s}^{-1}$ and $v_{\text{crit}} = 597 \text{ km s}^{-1}$. We also assume a CAK power-law index of $\alpha = \frac{1}{2}$ and cumulative line-strength parameter $\bar{Q} = 1533$ (Gayley 1995). The value of δ has been set to zero in all simulations.

In any case, for a given choice of the CAK power-law index α , we find that results are largely independent of the specific physical parameters when cast in appropriately scaled units, normalizing, for example, radius by the stellar radius R_* , velocity by the wind terminal velocity v_∞ (which in turn scales with the stellar surface escape speed), time by the characteristic flow time R_*/v_∞ , and mass-loss rate in terms of the classical (point star) CAK value given in equation (13). To facilitate comparison with the analytic nozzle analysis in §§ 2 and 3, we again choose $\alpha = \frac{1}{2}$ and plot all simulation results using the above scalings.

We further note that essentially all the key VH-1 results reported here were very well reproduced by a completely independent, simple dimensionless hydrodynamics code developed by one of us (A. F.; Feldmeier & Nikutta 2006). Finally, in such time-dependent simulations of line-driven winds, one must also supply a generalized scaling for the line force that applies in the case of nonmonotonic flow acceleration. In general this requires taking into account *nonlocal* couplings of the line transfer (see, e.g., Feldmeier & Nikutta 2006), but we wish here to retain the substantial advantages of using a purely local form for the line driving. Noting that a negative velocity gradient implies a prior line resonance that shadows radial photons from the star, a lower limit would be just to set $g_{\text{line}} = 0$ whenever $dv/dr < 0$. On the other hand, since forward scattering can substantially weaken any such shadowing by a prior resonance, an upper limit would be to compute the local line force using the absolute value of the velocity gradient, $g_{\text{line}} \propto |dv/dr|^\alpha$. As a simple compromise between these two extremes, we choose here a scaling that truncates the radial velocity gradient to zero whenever it is negative, i.e., $dv/dr \rightarrow \max(dv/dr, 0)$. For a point-star model with radially streaming radiation, this would give a zero line force (since $dv/dr < 0$), but when one accounts for the lateral expansion v/r within the FDCF, it leads to a line force in which the usual dependence on radial velocity gradient is replaced by a dependence on the expansion gradient,

$$g_{\text{line}} \propto \left(\frac{v}{r}\right)^\alpha. \quad (23)$$

This leads to a line acceleration that is intermediate between the underestimate and overestimate of the two more extreme scalings.

5. COMPARISON WITH TIME-DEPENDENT HYDRODYNAMIC SIMULATIONS

5.1. Asymptotic Steady States of Time-dependent Simulations

In our basic parameter study, each simulation is run using the same initial condition, spatial mesh, boundary conditions, base

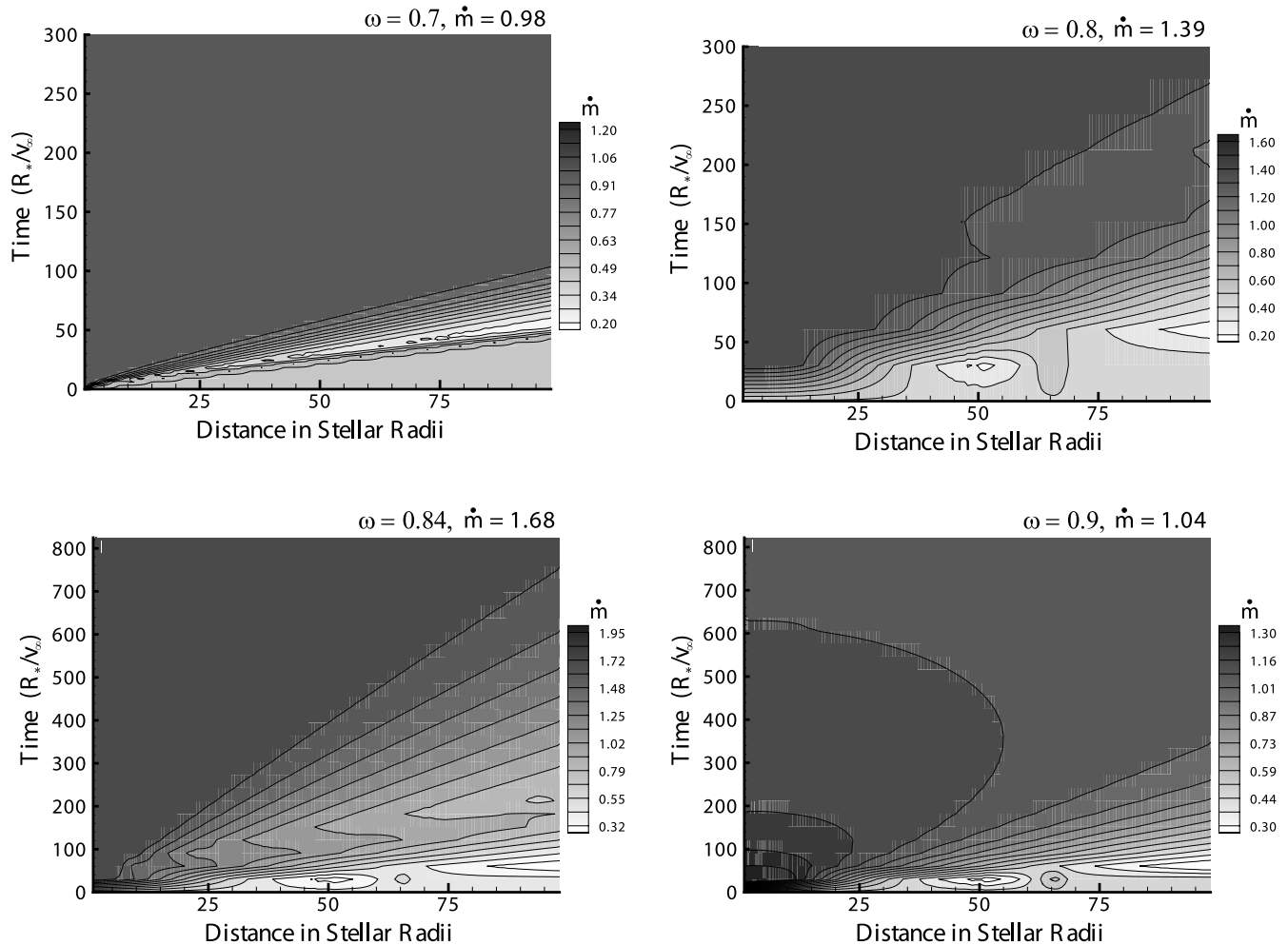


FIG. 5.—Gray-scale plots showing time evolution of mass-loss rate in units of the point-star CAK value. The corresponding rotation rate and final mass-loss rate are given above each plot. Time is in units of the flow time $t = R_*/v_\infty$. Note in each the eventual constancy of the mass-loss rate with both radius and time, indicating relaxation to a steady state solution. Note that the ranges for both gray scale and time differ for each panel.

density, etc., with the only variation being the rotation rate ω , which is set to specific values ranging from 0.1 to 0.97. With only one exception (for the $\omega = 0.85$ case, which turns to be a rather pathological value; see § 5.2), all simulations asymptotically relax to a well-defined steady state. Moreover, for both moderate rotation ($\omega < 0.75$) and high rotation ($\omega > 0.85$), these asymptotic states agree remarkably well with the predictions of the above nozzle analysis. Figure 3*b* shows the velocity laws for these final states, scaled in the same form used in Figure 3*a* for the nozzle-analysis results. Note that both Figures 3*a* and 3*b* show a steep acceleration for no or modest rotation ($\omega = 0-0.7$) and shallow acceleration for rapid, near-critical rotation ($\omega = 0.86, 0.9$, and 0.95).

However, for the moderately high rotation rate cases $\omega = 0.75, 0.8, 0.82$, and 0.84 , note also the appearance of a new class of *kink* solutions, characterized by an abrupt shift to a decelerating or “coasting” flow beyond a well-defined “kink radius” r_{kink} . These kink solutions thus represent a kind of intermediary final state of the time-dependent simulations in the parameter ranges $0.75 < \omega < 0.85$, effectively smoothing the abrupt jump from fast- to slow-acceleration solutions expected from steady state analyses. The formation of such kinks and their underlying physical cause are discussed further in the section below (§ 5.2) on time evolution.

Figure 4 shows that the fully dynamical results for the scaled ratio of right boundary speed (*circles*) and CAK-scaled mass-loss rate (*triangles*) are generally in good agreement with the

predictions of the simple nozzle analysis (*solid curves*), with the modest, ca. 10% differences likely attributable to inclusion in the simulations of a small but finite sound speed (Owocki and ud-Doula 2004). However, for rotation rates $0.75 < \omega < 0.85$, the dynamical results tend to follow the dashed curves of the extended nozzle analysis, representing extended fast solutions, rather than the abrupt shift to slow solutions, indicated by the solid curves. As discussed above, this range of rotation rates is characterized by kink solutions. To understand better this development of fast versus slow versus kink solutions, let us now examine the time evolution of the simulations toward asymptotic states.

5.2. Time Relaxation of 1D Rotation Models

For the specific rotation rates $\omega = 0.7, 0.8, 0.84$, and 0.90 , which span the parameter range between fast- and slow-acceleration solutions, Figure 5 uses gray-scale plots of the mass-loss rate (in units of the point-star CAK value) to illustrate the time relaxation from the CAK initial condition (set to a nonrotating, finite-disk corrected CAK model) to an asymptotic steady state. Time is given in units of the flow time $t = R_*/v_\infty$, and the final values of the scaled mass-loss rate are indicated above the associated plot. Note that there are distinct differences in the time evolution of each model, with the more rapid rotation cases characterized by a longer relaxation time, but the temporal and spatial constancy of

A NOZZLE ANALYSIS OF SLOW-ACCELERATION SOLUTIONS IN ONE-DIMENSIONAL MODELS OF ROTATING HOT-STAR WINDS

Thomas I. Madura and Stanley P. Owocki

Bartol Research Institute, Department of Physics and Astronomy, University of Delaware, Newark, DE 19716;
tmadura@udel.edu, owocki@bartol.udel.edu

and

Achim Feldmeier

Astrophysik, Institut für Physik, Universität Potsdam, Am Neuen Palais 10, 14469 Potsdam, Germany; afeld@astro.physik.uni-potsdam.de

Received 2006 September 1; accepted 2007 January 8

ABSTRACT

One-dimensional (1D) stellar wind models for hot stars rotating at 75% of the critical rate show a sudden shift to a slow-acceleration mode, implying a slower, denser equatorial outflow that might be associated with the dense equa-

